Highly Compressed Assembly of Deformable Nanogels into Nanoscale Suprastructures and Their Application in Nanomedicine

Huabing Chen,[†,‡,∥] Hongda Zhu,[†,‡,∥] Jingdong Hu,[†,‡] Yanbing Zhao,[†,‡] Qin Wang,[§] Jiangling Wan,[†,‡] Yajiang Yang,[§] Huibi Xu,[†,‡] and Xiangliang Yang[†,‡,⊥,*]

[†]College of Life Science and Technology, Huazhong University of Science and Technology, Wuhan 430074, China, [‡]National Engineering Research Center for Nanomedicine, Wuhan 430074, China, and [§]School of Chemistry and Chemical Engineering, Huazhong University of Science and Technology, Wuhan 430074, China [∥] These authors contributed equally to this work. [⊥] Present address: College of Life Science and Technology, Huazhong University of Science and Technology, Wuhan 430074, China.

ABSTRACT Assembly of nanoparticles as interfacial stabilizers at oil-in-water (O/W) interfaces into microscopic suprastructures for stabilizing Pickering emulsions is an intriguing focus in the fields of chemical industry and material sciences. However, it is still a major challenge to assemble nanoscale suprastructures using nanoparticles as building blocks at O/W interfaces for fabricating nanoscale emulsion droplets with applicable potential in nanomedicine. Here, we show that it is possible to fabricate the nanodroplets by assembling highly deformable nanogels into the nanoscale suprastructures at spatially confined O/W interfaces. The compressed assembly of the nanogels induced the formation of the nanoscale suprastructures upon energy input at the nanoscale O/W interface. The hydrogen bonding interaction between the nanogels at the O/W interface are possibly responsible for the stabilization of the nanoscale suprastructures. The nanoscale suprastructures are further employed to stabilize the paclitaxel-loaded nanodroplets, which are found to provide sustained release of the drug, enhanced *in vitro* cytotoxicity, and prolonged *in vivo* blood circulation. Furthermore, the tissue distribution and antitumor efficacy studies show that the nanodroplets could induce a higher drug accumulation at the tumor site and enhance tumor growth inhibition when compared with the commercial product. This approach provides a novel universal strategy to fabricate nanoscale suprastructures for stabilizing nanodroplets with built-in payloads using deformable nanoparticles and displays a promising potential in nanomedicine.

KEYWORDS: nanogels · nanoscale suprastructures · nanodroplets · paclitaxel · nanomedicine

INTRODUCTION

Pickering emulsion is an emulsion that is stabilized by solid particles residing between an oily phase and aqueous phase. The assembly of the nanoparticles such as silica, microgel, Au, and polystyrene nanoparticles into microscopic suprastructures at oil-in-water (O/W) interfaces for stabilizing Pickering emulsions has been studied as an intriguing focus in field of chemical industry and material sciences.[1−4] Because of the preferential residing of nanoparticles at O/W interfaces, the microscopic suprastructures consisting of nanoparticles provide significant advantages over amphiphilic molecules or copolymers with high drug loading, strong kinetic hindrance to droplet−droplet coalescence, tunable interfacial permeability, enhanced controlled release of therapeutic molecules, and so on.[4−8] It is highly valuable to explore the applicable potential of the suprastructures with these advantages in nanomedicine. However, the microscopic suprastructures consisting of these nanoparticles can only induce the formation and stabilization of microscopic emulsion droplets. It is difficult to fabricate nanoscale suprastructures for stabilizing nanoscale emulsion droplets using these nanoparticles, because the stronger interfacial hindrance is required to resist the droplet−droplet coalescence and the relatively higher interfacial curvature of nanodroplets can induce the spatially confined interface upon the formation of nanoscale emulsions.[9] Especially, the confined nanoscopic space at the O/W interface of nanodroplets does not allow nanoparticles to perfectly arrange at the O/W interface. Consequently, the intact assembly of nanoparticles into nanoscale suprastructures at the spatially confined space of O/W interfaces becomes the major challenge in the development of nanodroplets for nanomedicine.

Recently, ideas about the assembly of flexible DNA chains and porous nanoparticles into nanoarchitectures imply an intriguing strategy to fabricate the nanoarchitectures by using deformable or soft building blocks.[10−14]

* Address correspondence to yangxl@mail.hust.edu.cn.

Received for review October 26, 2010 and accepted March 4, 2011.

Published online March 04, 2011
10.1021/nn102888c

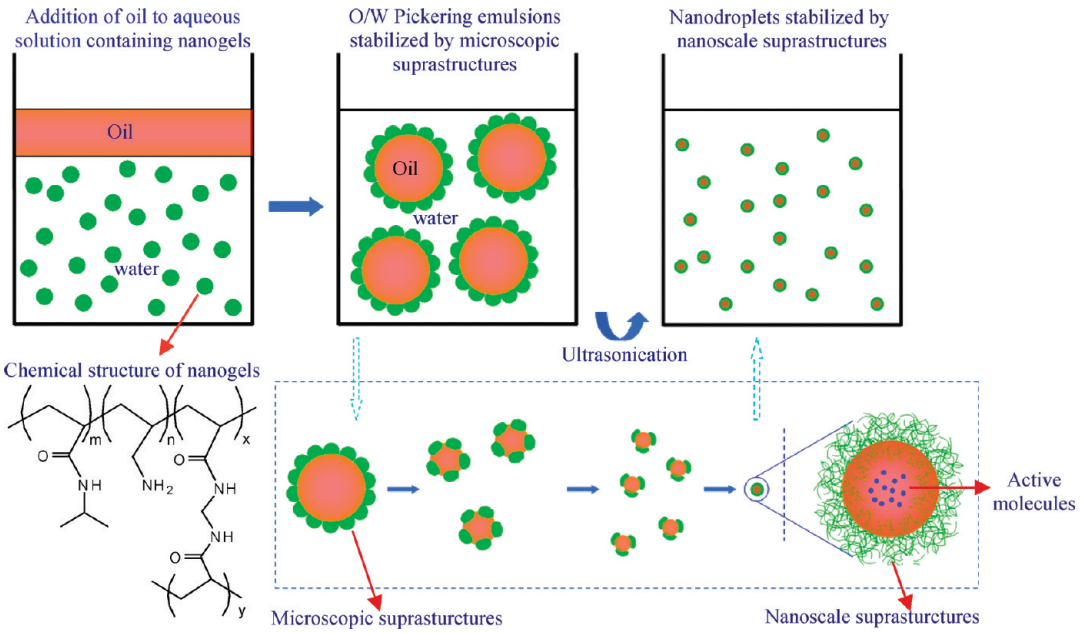

Figure 1. Schematic illustration of the highly compressed assembly of nanogels into the nanoscale suprastructures at O/W interfaces which are used to stabilize the nanodroplets with active molecules for nanomedicine.

The spherical poly(*N*-isopropylacrylamide) (PNIPAM)-based nanogels were found to have significant deformability of swelling−shrinkage in response to an external stimulus (e.g., temperature) in our previous studies,[15,16] and displayed different physicochemical properties from those of the solid nanoparticles.[7,17] The shrinkage capacity of the nanogels is expected to provide a possibility of achieving the compressed assembly of nanogels into the nanoscale suprastructures at O/W interfaces. Here, we synthesized poly(*N*-isopropylacrylamide-*co*-allylamine) (PNIPAM-*co*-AA) nanogels, where *N*-isopropylacrylamide was used as the scaffold of network-like nanogels with deformability.[15,16] Allylamine was copolymerized to improve the hydrophilicity of PNIPAM-based nanogels at 37 °C, because PNIPAM can display rapid dehydration above 32 °C.[18] The nanogels could first form microscopic suprastructures for stabilizing Pickering emulsions at O/W interfaces and further be compressed into nanoscale suprastructures upon energy input (e.g., ultrasonication) (Figure 1). The nanoscale suprastructures were further used to stabilize the nanodroplets with active molecules in the oily phase, which were further evaluated as the nanocarrier for cancer therapy.

RESULTS AND DISCUSSION

The PNIPAM-*co*-AA nanogels were synthesized using *N*-isopropylacrylamide and allylamine at a ratio of 7:1 (Supporting Information). The PNIPAM-*co*-AA nanogels with positive zeta potentials in aqueous solution displayed a significant size change from 188.4 nm at 28 °C to 67.5 nm at 42 °C (Figure S1a−c). The volume of the nanogels at 42 °C is only about 4.6% of that at 28 °C, which implies that the nanogels have significant shrinkage capability. The lyophilized PNIPAM-*co*-AA nanogels at the shrunken state were further found to have an average diameter of 48.4 nm using a field small-angle X-ray scattering system. TEM imaging also validated that the nanogels had a spherical morphology and were highly shrunken at 37 °C (Figure S1d and S1e). It reveals that the nanogels have a highly deformable ability *via* hydration or dehydration, which allows the nanogels to significantly swell or shrink in aqueous solution.[19] The shrinkage ability is expected to provide the nanogels with an ability to perfectly arrange at O/W interfaces in a spatially confined space.

To demonstrate the preferential distribution of the PNIPAM-*co*-AA nanogels at O/W interfaces, FITC as a fluorescent dye was conjugated to PNIPAM-*co*-AA nanogels *via* amide, which were first used to stabilize the microscopic suprastructures for stabilizing the Pickering emulsions droplets.[20,21] The hydrophobic organic solvents such as isopropyl myristate (IPM) and hexane could act as the oily phase of Pickering emulsions. FITC-labeled PNIPAM-*co*-AA nanogels were used to stabilize pharmaceutically acceptable IPM droplets. Fluorescent imaging showed that a yellow-green color existed around the droplets and was possibly ascribed to the FITC-labeled PNIPAM-*co*-AA nanogels around microscopic emulsion droplets (Figure 2a). Nile red (1.0 μg/mL) as a red hydrophobic fluorescent dye was encapsulated into oily droplets of the Pickering emulsions stabilized by the microscopic suprastructures of PNIPAM-*co*-AA nanogels. The red fluorescence from nile red validated the presence of spherical oily droplets inside the Pickering emulsions (Figure 2b). Furthermore, FITC-labeled PNIPAM-*co*-AA nanogels were used to stabilize the oily droplets containing

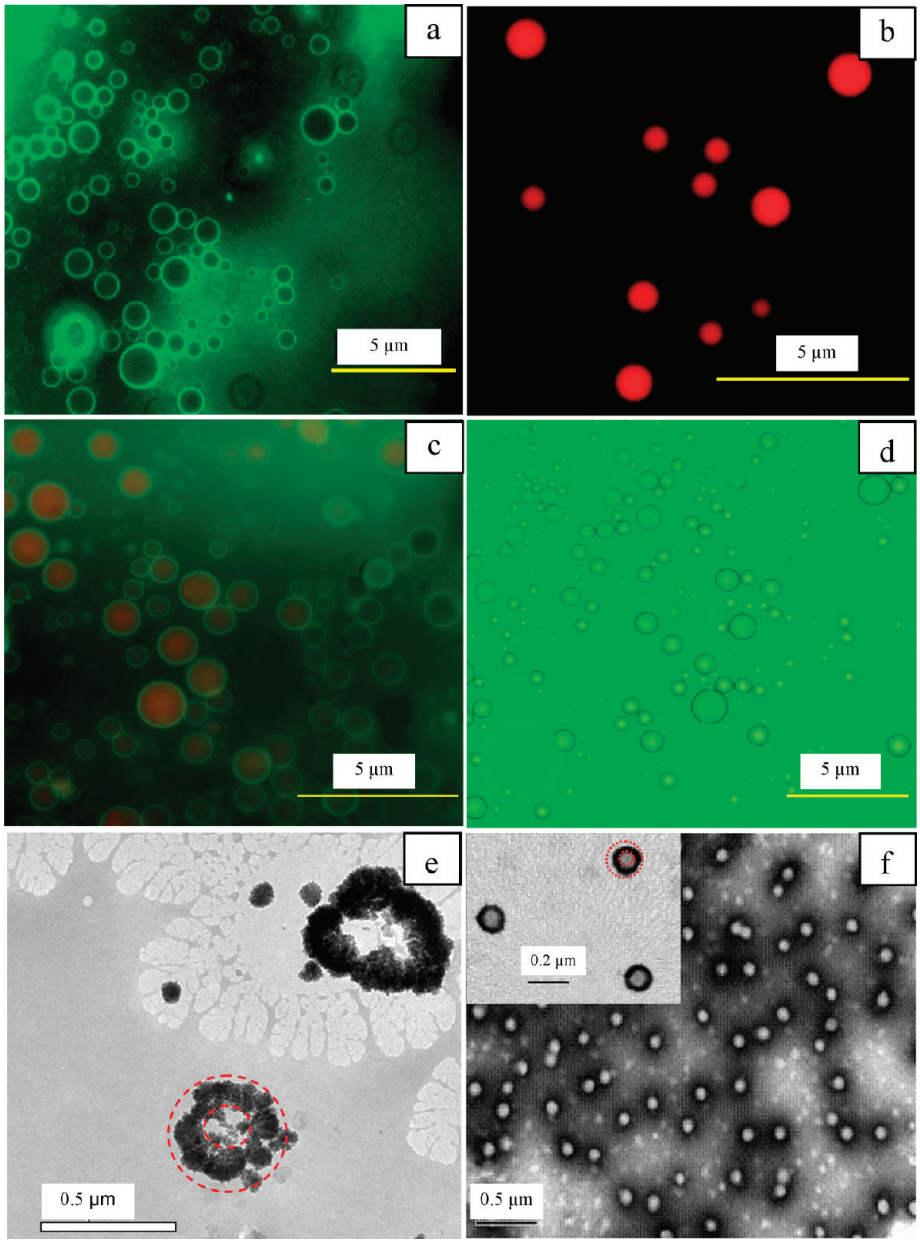

Figure 2. Fluorescent and TEM imaging of the Pickering emulsions and nanodroplets. (a) Fluorescent images of the Pickering emulsions stabilized by the microscopic suprastructures of FITC-labeled PNIPAM-*co*-AA nanogels. (b) Fluorescent image of the Pickering emulsions containing nile red, stabilized by the microscopic suprastructures of PNIPAM-*co*-AA nanogels. (c) Fluorescent image of the Pickering emulsions containing nile red, stabilized by the microscopic suprastructures of FITC-labeled PNIPAM-*co*-AA nanogels. (d) Optical image of the Pickering emulsion stabilized by the microscopic suprastructures of FITC-labeled PNIPAM-*co*-AA nanogels. (e) TEM images of the Pickering emulsions stabilized by the microscopic suprastructures of PNIPAM-*co*-AA nanogels (dashed circle indicates the capsule-like morphology). (f) TEM images of the nanodroplets stabilized by the nanoscale suprastructures of PNIPAM-*co*-AA nanogels (dashed circle indicates the capsule-like morphology).

nile red for differentiating the interfacial microscopic suprastructures and interior oily droplets (Figure 2c). The red fluorescence from nile red was observed in the interior of droplets, and simultaneously a yellow-green color from FITC-labeled PNIPAM-*co*-AA nanogels coexisted surrounding the droplets. It indicated that the microscopic suprastructures consisting of the nanogels located at O/W interfaces of the Pickering emulsions and could be differentiated from inner oily droplets. TEM imaging was further used to validate the droplet morphology of the microscopic Pickering emulsions.[22,23] Figure 2e and Figure S2a showed that the Pickering emulsions displayed a capsule-like structure, which implied that the microscopic suprastructures might surround the oily droplets and matched well with their fluorescent imaging and optical imaging (Figure 2d). But the microscopic Pickering emulsions had an average droplet size of 1.5 μm and a broad size distribution

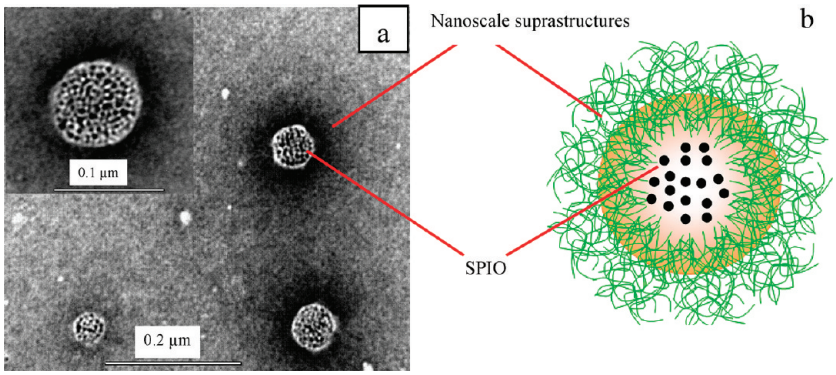

Figure 3. (a) TEM images of SPIO clusters stabilized by the nanoscale suprastructures (insert, same sample at various magnifications). (b) Schematic illustration of SPIO clusters stabilized by the nanoscale suprastructures of the PNIPAM-*co*-AA nanogels.

(polydispersive index is 0.396) (Figure S2b). Figure 2e also showed that the microscopic suprastructures around Pickering emulsion droplets had a thickness of 150−200 nm, which is comparable to the particle size of the nanogels at the swollen status in aqueous solution as shown in Figure S1a. In addition, the Pickering emulsions with a microscopic droplet size displayed a significant temperature-responsive size change (Figure S2c), which should be attributed to the temperature-responsive nanogels at O/W interfaces. Furthermore, the Pickering emulsions also avoided the phase separation of the emulsions at 37 °C due to the presence of the amino group in the nanogels.[7] Generally, the PNIPAM-based polymers can be dehydrated and display phase separation when the temperature is above 32 °C. The amine group from allylamine could prevent the nanogels from precipitation because of the enhancement of their hydrophilicity. It implies that the nanogels could display a state of dehydration at 37 °C and maintained amphiphilic properties at O/W interfaces as well, which was very important for their stability. Then, the nanogels can form the microscopic suprastructures as shown in Figure 1 and maintain their original size at O/W interfaces of the Pickering emulsions at room temperature and also afford the steric hindrance to droplet−droplet coalescence for the stabilization of Pickering emulsions.[4]

Interestingly, we found the presence of the nanoscale suprastructures at O/W interfaces when we further disintegrated the above emulsions into nanoscale emulsion droplets using ultrasonication (Figure 1). Figure 2f showed the TEM images of the nanodroplets stabilized by nanoscale suprastructures of PNIPAM-*co*-AA nanogels. The nanodroplets showed a capsule-like morphology that was similar to that of the above emulsions. But their droplet size was significantly decreased to about 137.0 nm and the thickness of nanoscale suprastructures only ranged from 30 to 60 nm (Figure 2f). This thickness was much lower than that of the microscopic suprastructures of the Pickering emulsions, and it was similar to the particle size of the shrunk nanogels (Figure S1a and S1e). The FITC-labeled PNIPAM-*co*-AA nanogels were used to construct fluorescent nanoscale suprastructures to stabilize the nanodroplets, and the fluorescence imaging (Figure S3) showed that the fluorescent morphology of nanodroplets was significantly different with that of Pickering emulsions stabilized by the microscopic suprastructures in Figure 2a because of their small diameters. In addition, the nanodroplets had a narrow size distribution (Figure S2d) and only showed a slight change of droplet size when the temperature was increased. The PNIPAM-*co*-AA nanogels at O/W interfaces might be significantly shrunken with the simultaneous expulsion of water from the interior gel network when the emulsion droplets were disintegrated by ultrasonication, even though no other stimulus (e.g., temperature) was applied. The ultrasonication might trigger the dehydration of the nanogels and subsequently induce the transformation of the microscopic suprastructures into nanoscale suprastructures when the PNIPAM-*co*-AA nanogels were forced to rearrange at O/W interfaces of the nanodroplets.

To validate the presence of the nanoscale suprastructures, we employed the nanodroplets as a template to encapsulate inorganic superparamagnetic iron oxide nanoparticles (SPIO) clusters using evaporable hexane containing hydrophobic SPIO as an oily phase and the nanoscale suprastructures as stabilizers (Supporting Information, Figure S4a and S4b).[3,24,25] Here, SPIO were used to differentiate the hydrophobic oily phase and nanoscale suprastructures because of their strong TEM imaging contrast (Figure S4a). The hydrophobic SPIO are expected to reveal the oily microstructure within the nanodroplets. TEM imaging in Figure 3a showed that tens of hydrophobic SPIO aggregated into the clusters with the diameters ranging from 50 to 100 nm, which were surrounded by the nanoscale suprastructures with a thickness of about 50 nm. The morphology and size (average diameter of 149.2 nm from DLS) of these nanoscale suprastructures were similar to those of the above nanodroplets. The SPIO clusters had a high relaxivity of 121.3 mM^{-1} s^{-1} (Figure S4c) and also

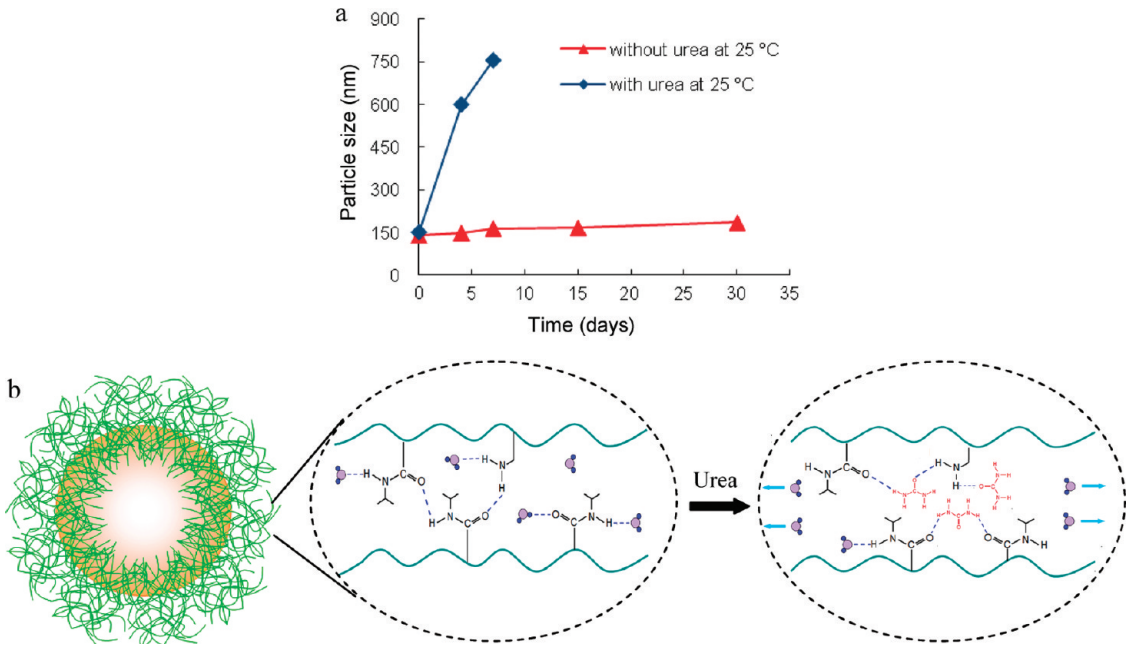

Figure 4. Validation of hydrogen bonds between the nanogels in the nanoscale suprastructures at O/W interfaces. (a) Influence of urea (4.0 mol/L) on the stability of the nanodroplets stabilized by the nanoscale suprastructures of PNIPAM-*co*-AA nanogels at 25 °C. (b) Proposed interaction mechanism of urea with side chains of the nanogels in the nanoscale suprastructures at O/W interfaces.

showed no significant change of particle size during 30 days (data is not shown), which implied that the nanoscale suprastructures exhibited good encapsulation and stabilization for hydrophibic SPIO clusters.[24,25] The formation and stabilization of SPIO clusters validated the presence of the nanoscale suprastructures at the O/W interface of nanodroplets as proposed in Figure 3b.

The compressed assembly of the nanogels into the nanoscale suprastructures during ultrasonication of the Pickering emulsions possibly attributed to the shrinkage of nanogels at O/W interfaces. According to the Young−Laplace equation for the spherical oil droplets in an O/W emulsion,[26]

$$\Delta P = \frac{2\gamma}{r}$$

(where ΔP is the pressure difference across the O/W interface, γ is the interfacial tension of the oil droplet, and r is the radius of the oil droplet). The proposed formation mechanism of the nanoscale suprastructures of PNIPAM-*co*-AA nanogels can be described as follows: Firstly, for the microscopic Pickering emulsions without a strong energy input (ΔP is kept constant), the thickness of the microscopic suprastructures of PNIPAM-*co*-AA nanogels at O/W interfaces was equal to the particle size of the nanogels at the swelling state. Then, the nanogels could form the interfacial layers at O/W interfaces for decreasing the interfacial tension at O/W interfaces. When the Pickering emulsions were disintegrated into the nanodroplets by ultrasonication, ΔP was increased by the input of ultrasonication energy, and the value of γ could not be decreased since the nanogels had located at O/W interfaces in the Pickering emulsions. So, the radius of the emulsion droplets have to be further decreased according to the equation. Consequently, the packing density or volume of nanogels adsorbed per unit area at O/W interfaces was significantly increased with the decrease in droplet size. The increase of their density or volume in the spatially confined space can trigger the squeeze and dehydation of the nanogels around droplets, because the input of power could overcome the osmotic pressure of the nanogels in the aqueous side of O/W interfaces and then lead to the release of water from the nanogels. Finally, the squeeze of the nanogels induced the formation of the nanoscale suprastructures and also allowed the nanogels to perfectly arrange around nanodroplets with relatively high interfacial curvature.

In order to explore the stabilization mechanism of the nanoscale suprastructures, we probed the presence of hydrogen bonding interaction between the nanogels at O/W interfaces using urea, which was used to break hydrogen bonds existing between the nanogels (Figure 4a and 4b).[18,27,28] Urea was expected to penetrate into the nanoscale suprastructures from the aqueous phase, effectively interact with the nanogels *via* hydrogen bonds, and break the existing hydrogen bonds between the nanogels.[27] The nanodroplets without urea only had a slight increase of droplet size during 30 days, but the addition of urea resulted in the quick coarsening of droplets after storage for 4 days and phase separation after 7 days at 25 or 37 °C (Figure 4a

and Figure S5). It shows that the hydrogen bond interaction is possibly one of the most important mechanisms for the stability of the nanoscale suprastructures. Additionally, we also found that the microscopic suprastructures formation of the Pickering emulsions hardly relied on the interaction of hydrogen bonds between the nanogels, but the nanoscale suprastructures for stabilizing the nanodroplets obviously depended on this interaction (Supporting Information). This interaction possibly induced the interlock of the nanogel network, which is advantageous to the perfect surface coverage of droplets with high interfacial curvature for avoiding droplet−droplet coalescence and the dissociation of the nanogels from the nanoscale suprastructures.[29,30]

The nanodroplets contain hydrophobic oily droplets stabilized by the nanoscale suprastructures, which possibly act as a reservoir for drug delivery in nanomedicine. In this work, paclitaxel as a hydrophobic anticancer drug was selected as the model drug to demonstrate the potential of the nanodroplets for cancer therapy. Paclitaxel has been encapsulated into several nanocarriers including albumin protein,[31] liposomes,[32] carbon nanoparticles,[33,34] polymeric micelles,[35] and nanoemulsion[36] for prolonging blood circulation time, decreasing adverse side effects, or improving antitumor efficacy. We prepared the paclitaxel-loaded nanodroplets stabilized by the nanoscale suprastructures (Supporting Information). The *in vitro* drug release behavior (Figure 5a) showed that paclitaxel from the control solution was quickly released into the release medium in which 1.0 mol/L sodium salicylate was used to maintain sink conditions. The nanodroplets showed the sustained release of paclitaxel from nanodroplets, which might be attributed to the controllable permeability of nanoscale suprastructures induced by the intact arrangement of the shrunk nanogels around the O/W interface.[4,7,37−39] It shows that the nanodroplets have excellent sustained release profiles of the drug from nanodroplets. We used the MTT method to evaluate the viability of A2780 cells after incubation with paclitaxel-loaded nanodroplets for 24 h. Paclitaxel was solubilized in 10% DMSO as a control group.[40,41] Figure 5b showed the relative cell viability of the paclitaxel-loaded nanodroplets. The paclitaxel-loaded nanodroplets had a significantly lower IC_{50} (5.0 μg/mL) value than free paclitaxel (12.5 μg/mL), which might be attributed to the good internalization of the nanodroplets by cells *via* an enhanced electrostatic interaction.[42] The paclitaxel-free nanodroplets showed no significant cytotoxicity. These results indicate that the encapsulation of paclitaxel by the nanoscale suprastructures in the nanodroplets plays an important role in the enhancement of cytotoxic activity.

The *in vivo* pharmacokinetic behavior and tissue distribution of the paclitaxel-loaded nanodroplets were further evaluated. Figure 5c and Table 1 showed the average plasma concentration−time curves and pharmacokinetic parameters of paclitaxel-loaded nanodroplets and commercial Taxol. The area under the curve ($AUC_{0\sim\infty}$) value of paclitaxel-loaded nanodroplets after intravenous administration was 4.9 times higher than that of Taxol. The nanodroplets showed a longer elimination half-life ($t_{1/2\beta}$) of 23.0 h when compared with that of Taxol (3.3 h). The $t_{1/2\beta}$ value was also much higher than that of commercial PEG-PLA micelles[35] and similar to that of other polyester-based nanoparticles decorated with PEG.[43,44] The prolonged $t_{1/2\beta}$ might be attributed to the sustained release of paclitaxel, avoidance of the rapid clearance by the reticulo-endothelial system, and rapid degradation of droplets induced by lipase.[45] It indicates that the nanoscale suprastructures provided a long blood circulation effect and good stability in blood circulation for the paclitaxel-loaded nanodroplets. It also implies that the nanoscale suprastructures can act as an alternative to polyethylene glycol for achieving a long circulation effect. Figure 5d showed that the concentrations of paclitaxel from the paclitaxel-loaded nanodroplets in a tumor were respectively increased by 20 and 8 times after 1 and 8 h postadministration when compared with those from Taxol. The nanodroplets induced much higher accumulations of drug at the tumor site when compared with the reported PEG-PLA micelles,[35] which might be attributed to the enhanced permeability retention (EPR) effect and longer half-life time of the nanodroplets. The high accumulation at the tumor site implied that the nanodroplets might achieve the passive targeting for paclitaxel delivery via the EPR effect.[46] The nanodroplets also exhibited high accumulation in liver after 1 and 8 h postadministration (Figure 5e and 5f). The higher levels of paclitaxel in liver reflected their role as main clearance routes for the paclitaxel-loaded nanodroplets, and the lower distribution at the other tissues implied the possibility of decreasing potential adverse side effects.[47] We further compared the antitumor effect of paclitaxel-loaded nanodroplets with that of Taxol in the ovarian carcinoma A2780 subcutaneous model at a dose of 10.0 mg/kg.[48] The paclitaxel-loaded nanodroplets (10.0 mg/kg) suppressed A2780 tumor growth from day 1 to 15 significantly (Figure 5g). At day 15, the control tumors reached a volume of 262.5 ± 74.0 mm^3. The tumors treated with the nanodroplets and Taxol had the volumes of 32.8 ± 7.5 mm^3 and 73.4 ± 21.3 mm^3, respectively. The nanodroplets displayed a much stronger tumor regression when compared with Taxol ($P < 0.01$). The longer half-life time and higher accumulation of paclitaxel at the tumor site possibly contributed to the enhanced antitumor effects. It indicates that the nanodroplets have a comparable or preferable antitumor efficacy to the existing nanocarriers such as PEG-PLA, liposomes, and carbon nanoparticles.[34,35] The nanodroplets could achieve passive targeting via enhanced EPR effect. Additionally, the presence of an

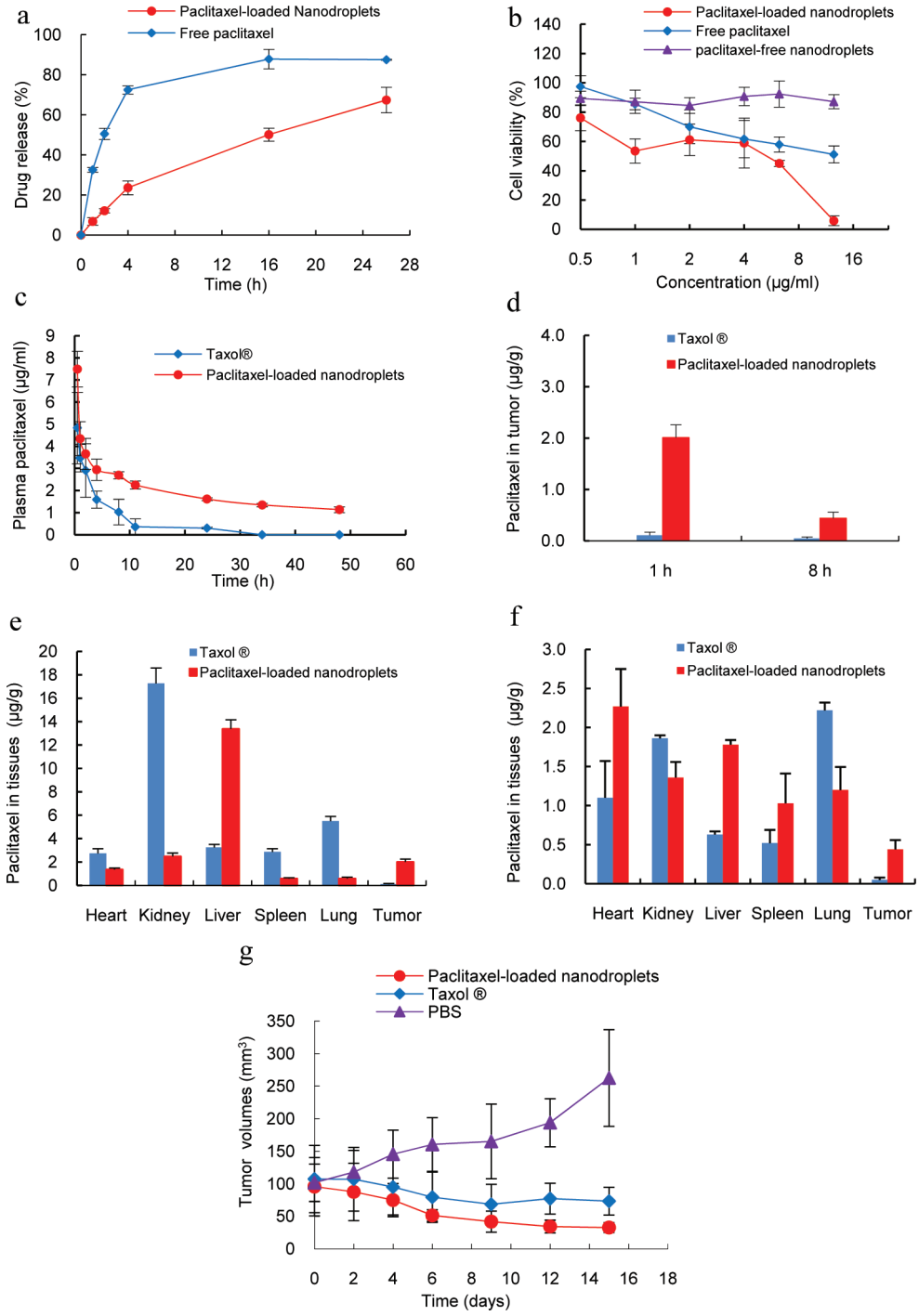

Figure 5. Drug release, cell viability, pharmacokinetic profiles, tissue distribution, and *in vivo* antitumor efficacy of the paclitaxel-loaded nanodroplets stabilized by the nanoscale suprastructures of PNIPAM-*co*-AA nanogels. (a) Release profiles of paclitaxel from the nanodroplets and control solution (n = 3). (b) Viability of A2780 cells after treatment with free paclitaxel, paclitaxel-loaded nanodroplets, and paclitaxel-free nanodroplets for 24 h. (c) Concentrations of paclitaxel in rat plasma at different times after intravenous administration of the paclitaxel-loaded nanodroplets and Taxol at the dose of 10 mg/kg. (d) Concentration of paclitaxel in tumors at 1 and 8 h after administration of the paclitaxel-loaded nanodroplets and Taxol at the dose of 10 mg/kg. (e) Concentrations of paclitaxel in heart, kidney, liver, spleen, lung, and tumor of mice treated at 1 h after administration of the paclitaxel-loaded nanodroplets and Taxol at the dose of 10 mg/kg. (f) Concentrations of paclitaxel in heart, kidney, liver, spleen, lung, and tumor of mice treated at 8 h after administration of the paclitaxel-loaded nanodroplets and Taxol at the dose of 10 mg/kg. (g) Tumor growth inhibition of the paclitaxel-loaded nanodroplets and Taxol on female athymic nude mice bearing subcutaneous A2780 xenografts after administration of 10 mg/kg (n = 6; the injections were performed on day 0, 4, and 8 for treatment).

amino group in the nanogels can also used for conjugation with some amino-reactive targeting ligand for active targeting in the future. It shows that the nanoscale suprastructure-stabilized nanodroplets

TABLE 1. Pharmacokinetic Parameters Observed in Rats after Intravenous Administration of Paclitaxel-Loaded Nanodroplets and Taxol at a Dose of 10 mg/kg (n = 5)

Parameters[a]	Paclitaxel-loaded nanodroplets	Taxol
$t_{1/2\beta}$ (h)	23.0 ± 3.3	3.3 ± 1.5
CL (L/h/kg)	0.07 ± 0.01	0.37 ± 0.09
$AUC_{0\text{-}t}$ (mg·h/mL)	96.24 ± 3.47	25.58 ± 6.75
$AUC_{0\text{-}\infty}$ (mg·h/mL)	138.55 ± 12.04	28.48 ± 7.64

[a] $t_{1/2\beta}$, elimination half life; AUC, area under the plasma concentration−time curve; CL, total body clearance.

display an intriguing potential for cancer therapy in nanomedicine.

In conclusion, the use of the deformable nanogels overcomes the key limitation of the fabrication of nanodroplets by allowing the straightforward compressed assembly of the nanogels into the nanoscale suprastructures at spatially confined O/W interfaces. The interaction of hydrogen bonds between the nanogels at O/W interfaces is possibly responsible for the stabilization of the nanoscale suprastructures. The intact nanoscale suprastructures provide a significant sustained release, enhanced *in vitro* cytotoxicity, and prolonged *in vivo* blood circulation, which triggered the enhanced drug accumulation in tumor site and improved tumor growth inhibition for paclitaxel-loaded nanodroplets. The nanoscale suprastructures can translate the Pickering emulsions into nanodroplets, which could provide some intriguing physicochemical and biological properties for cancer therapy. The present strategy provides a new means to fabricate nanoparticles and opens up a promising route for their application in nanomedicine.

METHODS

Preparation of Pickering Emulsions and Nanodroplets. The aqueous phases of nanogels were obtained by dissolving PNIPAM-co-AA into ultrapure water at 4 °C overnight. Isopropyl myristate (IPM) as an oily phase was mixed with the aqueous phase. The Pickering emulsions stabilized by 1% PNIPAM-co-AA nanogels were prepared by shearing the mixture of two phases at 13 000 rpm for 10 min (Fluko FA25 homogenizer). Cooling water was used to avoid an increase of temperature during the preparation. Finally, 10 mL Pickering emulsions consisted of 9% IPM, 1% nanogels, and water. The nanodroplets were further prepared by ultrasonicating the above emulsions into the nanoscale emulsions (400 W, 5 s: 5 s, 20 times) in an ice bath. The FITC-labeled PNIPAM-co-AA nanogels (Supporting Information) were used to prepare the fluorescent emulsions stabilized for validating the location of nanogels in Pickering emulsions according to the above method. For the encapsulation of nile red in the Pickering emulsions, nile red was dissolved in IPM to form the nile red oily phase, and then the Pickering emulsions (1.0 μg/mL nile red) stabilized by 1% PNIPAM-co-AA nanogels were prepared according to the above method. No significant influence of ultrasonication on the particle size of the nanogels was observed.

Particle Size Measurement. The average diameters of the samples were measured by dynamic laser scattering (DLS) (Nano ZS90, Malvern Instruments, U.K.) at 633 nm. The measurements were performed at different temperatures using a He−Ne laser. Additionally, in order to measure the particle size of shrunken nanogels, the nanogels were dissolved in water and then were lyophilized. Then, the lyophilized nanogels were analyzed using a field small-angle X-ray scattering system (Nanostar-C, Bruker-AXS), and the particle size was calculated using Guinier model.

Optical and Fluorescence Imaging. The Pickering emulsions stabilized by the microscopic suprastructures of the FITC-labeled PNIPAM-*co*-AA nanogels with or without nile red in oily phase were observed using an optical and fluorescence microscope (OLYMPUS IX-70). The nanodroplets stabilized by the nanoscale suprastructures of the FITC-labeled PNIPAM-*co*-AA nanogels were also observed using a fluorescence microscope. All the emulsions and nanodroplets were diluted using water before observation. Fluorescence imaging was performed at the excitation and emission wavelengths of 490 nm and 525 nm, respectively.

TEM Imaging. TEM imaging was used to probe the morphology of the Pickering emulsion droplets, nanodroplets, and SPIO clusters. The droplets were placed on a carbon-coated copper grid and dried in air. Then a solution of phosphotungstic acid (1%) was used to cover the samples, and the superfluous phosphotungstic acid was wiped off by filter paper, followed by being dried in air. Then dried samples were observed using Tecnai G2 20 TEM (FEI Corp., Netherlands) at 180 kV. The stained nanogels in TEM imaging displayed dark.[49]

Cell Viability. Ovarian carcinoma A2780 cells were grown in an RPMI-1640 medium with 10% (v/v) fetal bovine serum and 100 IU/mL of penicillin G sodium and 100 μg/mL of streptomycin sulfate. The cells were maintained in an incubator at 37 °C. A2780 cells were seeded in 96-well plates with a density of 4000 viable cells per well and incubated for 24 h for cell attachment. The cells were then incubated with free paclitaxel in 10% DMSO, paclitaxel-loaded nanodroplets, and paclitaxel-free nanodroplets for 24 h. Then, the formulations were replaced with RPMI-1640 containing MTT (10 μL, 5.0 mg/mL), and the cells were then incubated for an additional 4 h. MTT was aspirated off, and DMSO was added to dissolve the formazan crystals. The absorbance was measured at 490 nm using a PE Victor1420 (USA, Perkin-Elmer). The results were expressed as mean values ± standard deviation of 8 measurements. IC_{50} values were determined as the paclitaxel concentration where the relative cell viability was 50% of the untreated control cells.

Pharmacokinetic Study. The pharmacokinetics of paclitaxel-loaded nanodroplets was studied using Wistar rats weighing 220 ± 20 g. The animals were divided into two groups each of five rats and were further injected intravenously with 10 mg/kg paclitaxel-loaded nanodroplets and 10 mg/kg Taxol through the tail veins, respectively. A 0.4 mL aliquot of blood sample was collected from the orbital plexus of each rat into polyethylene cannulas at 0.5, 1, 2, 4, 8, 11, 24, 34, and 48 h. All the polyethylene cannulas were flushed with heparin to prevent blood clotting. The samples were centrifuged to collect plasma and stored at −70 °C. The concentrations of paclitaxel in rat plasma were determined using an HPLC system. 30 μL norethisterone (25.0 μg/mL in methanol) as the internal standard and 2 mL dichloromethane were added to the blood samples, and the mixtures were vortexed for 4 min and centrifuged at 4500 rpm for 10 min. The subnatants were collected and dried using nitrogen at 35 °C. Then, 200 μL of methanol were added to dissolve each dried sample for HPLC analysis. HPLC analysis was performed using an Agilent 1100 system with a Hypersil ODS column (5 μm, 4.6 mm × 250 mm) at 30 °C. The wavelength of paclitaxel was set at 227 nm. The mobile phase consisted of acetonitrile, methanol, and water (40:20:40) at a flow rate of 1.0 mL/min. The pharmacokinetic parameters were calculated using DAS 2.0 software.

Tissue Distribution. Taxol and paclitaxel-loaded nanodroplets were injected into tumor-bearing mice through a tail vein at a single dose of 10 mg/kg. At different time intervals after injection (1 and 8 h), the mice were sacrificed and the tumor, heart, liver, spleen, lung, and kidney were excised. Physiological

saline (2 mL) was added to each sample. The samples were further homogenized, and 4 mL of *tert*-butyl methyl ether were added. Subsequently, the samples were vortexed for 4 min, followed by centrifuging at 5000 rpm for 10 min. The supernatants were collected and dried using nitrogen at 35 °C. Then, 200 μL of methanol were added to dissolve each dried sample for HPLC analysis.

Tumor Growth Inhibition. The animal model of human ovarian carcinoma xenografts of Balb/c-nu/nu nude mice (5−7 weeks, 16−20 g) was used.[50] Briefly, A2780 human ovarian cancer cells (4×10^6) were subcutaneously transplanted into the flanks of female athymic nude (nu/nu) mice. When the tumors reached a size of ~100 mm^3 (15−20 days after transplantation), the mice were injected intravenously through the tail vein with PBS, Taxol, and paclitaxel-loaded nanodroplets at a dose of 10 mg/kg on day 0, 4, and 8, respectively. The tumor size was measured to evaluate the antitumor activity of various groups. The tumor volume (V) was calculated as follows: $V = L \times W^2/2$, where W is the tumor measurement at the widest point, and L is the tumor dimension at the longest point. The mice were sacrificed by cervical dislocation under an anesthetic status after the experiments. The statistic difference was analyzed using t tests where P values of <0.05 were considered significant.

Acknowledgment. This work was supported by the MOST 973 programs (Grant No. 2007CB935802 and 2010CB934000) of the Ministry of Science and Technology of China. The authors thank Prof. Stephen Z. D. Cheng at University of Akron, USA, Prof. Yuliang Zhao at Institute of High Energy Physics, Chinese Academy of Sciences, China, and Prof. Y. I. Chang at Tunghai University, Taiwan, for their helpful discussions. We thank the Analytical and Testing Center of Huazhong University of Science and Technology for the TEM analysis.

Supporting Information Available: Experimental details include synthesis of nanogels, validation of morphology, hydrogen bonding interactions of nanodroplets, and the release of paclitaxel from nanodroplets. This material is available free of charge via the Internet at http://pubs.acs.org.

REFERENCES AND NOTES

1. Madueno, R.; Raisanen, M. T.; Silien, C.; Buck, M. Functionalizing Hydrogen-Bonded Surface Networks with Self-Assembled Monolayers. *Nature* **2008,** *454*, 618–621.
2. Binder, W. H. Supramolecular Assembly of Nanoparticles at Liquid-Liquid Interfaces. *Angew. Chem., Int. Ed.* **2005,** *44*, 5172–5175.
3. Shenhar, R.; Rotello, V. M. Nanoparticles: Scaffolds and Building Blocks. *Acc. Chem. Res.* **2003,** *36*, 549–561.
4. Miller, R.; Fainerman, V. B.; Kovalchuk, V. I.; Grigoriev, D. O.; Leser, M. E.; Michel, M. Composite Interfacial Layers Containing Micro-Size and Nano-Size Particles. *Adv. Colloid Interface Sci.* **2006,** *128*, 17–26.
5. Dinsmore, A. D.; Hsu, M. F.; Nikolaides, M. G.; Marquez, M.; Bausch, A. R.; Weitz, D. A. Colloidosomes: Selectively Permeable Capsules Composed of Colloidal Particles. *Science* **2002,** *298*, 1006–1009.
6. Chen, H.; Khemtong, C.; Yang, X.; Chang, X.; Gao, J. Nanonization Strategies for Poorly Water-Soluble Drugs. *Drug Discovery Today*, in press, doi:10.1016/j.drudis.2010.02.009.
7. Berger, S.; Zhang, H. P.; Pich, A. Microgel-Based Stimuli-Responsive Capsules. *Adv. Funct. Mater.* **2009,** *19*, 554–559.
8. Simovic, S.; Prestidge, C. A. Nanoparticle Layers Controlling Drug Release from Emulsions. *Eur. J. Pharm. Biopharm.* **2007,** *67*, 39–47.
9. Myers, D. *Surfaces, Interfaces and Colloids*, 2nd ed.; Wiley & Sons: New York, 1999; pp 140−150.
10. Carr, R.; Weinstock, I. A.; Sivaprasadarao, A.; Muller, A.; Aksimentiev, A. Synthetic Ion Channels Via Self-Assembly: A Route for Embedding Porous Polyoxometalate Nanocapsules in Lipid Bilayer Membranes. *Nano Lett.* **2008,** *8*, 3916–3921.
11. Kraft, D. J.; Vlug, W. S.; van Kats, C. M.; van Blaaderen, A.; Imhof, A.; Kegel, W. K. Self-Assembly of Colloids with Liquid Protrusions. *J. Am. Chem. Soc.* **2009,** *131*, 1182–1186.
12. Douglas, S. M.; Dietz, H.; Liedl, T.; Hogberg, B.; Graf, F.; Shih, W. M. Self-Assembly of DNA into Nanoscale Three-Dimensional Shapes. *Nature* **2009,** *459*, 414–418.
13. Sharma, J.; Chhabra, R.; Cheng, A.; Brownell, J.; Liu, Y.; Yan, H. Control of Self-Assembly of DNA Tubules through Integration of Gold Nanoparticles. *Science* **2009,** *323*, 112–116.
14. Cheng, W.; Park, N.; Walter, M. T.; Hartman, M. R.; Luo, D. Nanopatterning Self-Assembled Nanoparticle Superlattices by Moulding Microdroplets. *Nat. Nanotechnol.* **2008,** *3*, 682–690.
15. Wang, Q.; Zhao, Y.; Xu, H.; Yang, X.; Yang, Y. Thermosensitive Phase Transition Kinetics of Poly (N-Isopropylacryl Amide-*Co*-Acrylamide) Microgel Aqueous Dispersions. *J. Appl. Polym. Sci.* **2009,** *113*, 321–326.
16. Wang, Q.; Xu, H.; Yang, X.; Yang, Y. Drug Release Behavior from in Situ Gelatinized Thermosensitive Nanogel Aqueous Dispersions. *Int. J. Pharm.* **2008,** *361*, 189–193.
17. Brugger, B.; Rutten, S.; Phan, K.-H.; Moller, M.; Richtering, W. The Colloidal Suprastructure of Smart Microgels at Oil-Water Interfaces. *Angew. Chem., Int. Ed.* **2009,** *48*, 3978–3981.
18. Burba, C. M.; Carter, S. M.; Meyer, K. J.; Rice, C. V. Salt Effects on Poly(N-Isopropylacrylamide) Phase Transition Thermodynamics from NMR Spectroscopy. *J. Phys. Chem. B* **2008,** *112*, 10399–10404.
19. Griset, A. P.; Walpole, J.; Liu, R.; Gaffey, A.; Colson, Y. L.; Grinstaff, M. W. Expansile Nanoparticles: Synthesis, Characterization, and in Vivo Efficacy of an Acid-Responsive Polymeric Drug Delivery System. *J. Am. Chem. Soc.* **2009,** *131*, 2469–2471.
20. Liu, B.; Wei, W.; Qu, X. Z.; Yang, Z. H. Janus Colloids Formed by Biphasic Grafting at a Pickering Emulsion Interface. *Angew. Chem., Int. Ed.* **2008,** *47*, 3973–3975.
21. Li, Z.; Ming, T.; Wang, J.; Ngai, T. High Internal Phase Emulsions Stabilized Solely by Microgel Particles. *Angew. Chem., Int. Ed.* **2009,** *48*, 8490–8493.
22. Walther, A.; Hoffmann, M.; Muller, A. H. E. Emulsion Polymerization Using Janus Particles as Stabilizers. *Angew. Chem., Int. Ed.* **2008,** *47*, 711–714.
23. Sacanna, S.; Kegel, W. K.; Philipse, A. P. Thermodynamically Stable Pickering Emulsions. *Phys. Rev. Lett.* **2007,** *98*, 158301.
24. Guthi, J. S.; Yang, S.-G.; Huang, G.; Li, S.; Khemtong, C.; Kessinger, C. W.; Peyton, M.; Minna, J. D.; Brown, K. C.; Gao, J. MRI-Visible Micellar Nanomedicine for Targeted Drug Delivery to Lung Cancer Cells. *Mol. Pharmaceutics* **2009,** *7*, 32–40.
25. Ai, H.; Flask, C.; Weinberg, B.; Shuai, X.-T.; Pagel, M. D.; Farrell, D.; Duerk, J.; Gao, J. Magnetite-Loaded Polymeric Micelles as Ultrasensitive Magnetic-Resonance Probes. *Adv. Mater.* **2005,** *17*, 1949–1952.
26. Shaw, D. *Introduction to Colloid and Surface Chemistry*, 4th ed.; Butterworth-Heinemann: 1992; pp 64−75.
27. Sagle, L. B.; Zhang, Y.; Litosh, V. A.; Chen, X.; Cho, Y.; Cremer, P. S. Investigating the Hydrogen-Bonding Model of Urea Denaturation. *J. Am. Chem. Soc.* **2009,** *131*, 9304–9310.
28. Hua, L.; Zhou, R.; Thirumalai, D.; Berne, B. J. Urea Denaturation by Stronger Dispersion Interactions with Proteins Than Water Implies a 2-Stage Unfolding. *Proc. Natl. Acad. Sci. U.S.A.* **2008,** *105*, 16928–16933.
29. Hanson, J. A.; Chang, C. B.; Graves, S. M.; Li, Z. B.; Mason, T. G.; Deming, T. J. Nanoscale Double Emulsions Stabilized by Single-Component Block Copolypeptides. *Nature* **2008,** *455*, 85–88.
30. Reincke, F.; Kegel, W. K.; Zhang, H.; Nolte, M.; Wang, D. Y.; Vanmaekelbergh, D.; Mohwald, H. Understanding the Self-Assembly of Charged Nanoparticles at the Water/Oil Interface. *Phys. Chem. Chem. Phys.* **2006,** *8*, 3828–3835.
31. Gradishar, W. J.; Tjulandin, S.; Davidson, N.; Shaw, H.; Desai, N.; Bhar, P.; Hawkins, M.; O'Shaughnessy, J. Phase III Trial of Nanoparticle Albumin-Bound Paclitaxel Compared with Polyethylated Castor Oil-Based Paclitaxel in Women with Breast Cancer. *J. Clin. Oncol.* **2005,** *23*, 7794–7803.
32. Crosasso, P.; Ceruti, M.; Brusa, P.; Arpicco, S.; Dosio, F.; Cattel, L. Preparation, Characterization and Properties of Sterically Stabilized Paclitaxel-Containing Liposomes. *J. Controlled Release* **2000,** *63*, 19–30.

33. Berlin, J. M.; Leonard, A. D.; Pham, T. T.; Sano, D.; Marcano, D. C.; Yan, S.; Fiorentino, S.; Milas, Z. L.; Kosynkin, D. V.; Price, B. K.; Lucente-Schultz, R. M.; Wen, X.; Raso, M. G.; Craig, S. L.; Tran, H. T.; Myers, J. N.; Tour, J. M. Effective Drug Delivery, in Vitro and in Vivo, by Carbon-Based Nanovectors Noncovalently Loaded with Unmodified Paclitaxel. *ACS Nano* **2010,** *4*, 4621–4636.
34. Zhan, C.; Gu, B.; Xie, C.; Li, J.; Liu, Y.; Lu, W. Cyclic RGD Conjugated Poly(Ethylene Glycol)-co-Poly(Lactic Acid) Micelle Enhances Paclitaxel Anti-Glioblastoma Effect. *J. Controlled Release* **2010,** *143*, 136–142.
35. Kim, S. C.; Kim, D. W.; Shim, Y. H.; Bang, J. S.; Oh, H. S.; Kim, S. W.; Seo, M. H. In Vivo Evaluation of Polymeric Micellar Paclitaxel Formulation: Toxicity and Efficacy. *J. Controlled Release* **2001,** *72*, 191–202.
36. Rapoport, N. Y.; Kennedy, A. M.; Shea, J. E.; Scaife, C. L.; Nam, K. H. Controlled and Targeted Tumor Chemotherapy by Ultrasound-Activated Nanoemulsions/Microbubbles. *J. Controlled Release* **2009,** *138*, 268–276.
37. Lee, D.; Weitz, D. A. Double Emulsion-Templated Nanoparticle Colloidosomes with Selective Permeability. *Adv. Mater.* **2008,** *20*, 3498–3503.
38. Kim, J.-W.; Fernandez-Nieves, A.; Dan, N.; Utada, A. S.; Marquez, M.; Weitz, D. A. Colloidal Assembly Route for Responsive Colloidosomes with Tunable Permeability. *Nano Lett.* **2007,** *7*, 2876–2880.
39. Tsuji, S.; Kawaguchi, H. Thermosensitive Pickering Emulsion Stabilized by Poly(N-Isopropylacrylamide)-Carrying Particles. *Langmuir* **2008,** *24*, 3300–3305.
40. Onyuksel, H.; Jeon, E.; Rubinstein, I. Nanomicellar Paclitaxel Increases Cytotoxicity of Multidrug Resistant Breast Cancer Cells. *Cancer Lett* **2009,** *274*, 327–330.
41. Devalapally, H.; Duan, Z. F.; Seiden, M. V.; Amiji, M. M. Modulation of Drug Resistance in Ovarian Adenocarcinoma by Enhancing Intracellular Ceramide Using Tamoxifen-Loaded Biodegradable Polymeric Nanoparticles. *Clin. Cancer Res.* **2008,** *14*, 3193–3203.
42. Arvizo, R. R.; Miranda, O. R.; Thompson, M. A.; Pabelick, C. M.; Bhattacharya, R.; Robertson, J. D.; Rotello, V. M.; Prakash, Y. S.; Mukherjee, P. Effect of Nanoparticle Surface Charge at the Plasma Membrane and Beyond. *Nano Lett.* **2010,** *10*, 2543–2548.
43. Dong, Y.; Feng, S. S. In Vitro and in Vivo Evaluation of Methoxy Polyethylene Glycol-Polylactide (MPEG-PLA) Nanoparticles for Small-Molecule Drug Chemotherapy. *Biomaterials* **2007,** *28*, 4154–4160.
44. Win, K. Y.; Feng, S. S. In Vitro and in Vivo Studies on Vitamin E TPGS-Emulsified Poly(D,L-Lactic-co-Glycolic Acid) Nanoparticles for Paclitaxel Formulation. *Biomaterials* **2006,** *27*, 2285–2291.
45. Tang, N.; Du, G.; Wang, N.; Liu, C.; Hang, H.; Liang, W. Improving Penetration in Tumors with Nanoassemblies of Phospholipids and Doxorubicin. *J. Natl. Cancer Inst.* **2007,** *99*, 1004–1015.
46. van Vlerken, L. E.; Duan, Z.; Little, S. R.; Seiden, M. V.; Amiji, M. M. Biodistribution and Pharmacokinetic Analysis of Paclitaxel and Ceramide Administered in Multifunctional Polymer-Blend Nanoparticles in Drug Resistant Breast Cancer Model. *Mol Pharmaceut.* **2008,** *5*, 516–526.
47. Blanco, E.; Bey, E. A.; Khemtong, C.; Yang, S.-G.; Setti-Guthi, J.; Chen, H.; Kessinger, C. W.; Carnevale, K. A.; Bornmann, W. G.; Boothman, D. A.; Gao, J. β-Lapachone Micellar Nanotherapeutics for Non-Small Cell Lung Cancer Therapy. *Cancer Res.* **2010,** *70*, 3896–3904.
48. Andrew MacKay, J.; Chen, M.; McDaniel, J. R.; Liu, W.; Simnick, A. J.; Chilkoti, A. Self-Assembling Chimeric Polypeptide-Doxorubicin Conjugate Nanoparticles That Abolish Tumours after a Single Injection. *Nat. Mater.* **2009,** *8*, 993–999.
49. Zhang, F.; Wang, C.-C. Preparation of P(NIPAM-co-AA) Microcontainers Surface-Anchored with Magnetic Nanoparticles. *Langmuir* **2009,** *25*, 8255–8262.
50. Dharap, S. S.; Wang, Y.; Chandna, P.; Khandare, J. J.; Qiu, B.; Gunaseelan, S.; Sinko, P. J.; Stein, S.; Farmanfarmaian, A.; Minko, T. Tumor-Specific Targeting of an Anticancer Drug Delivery System by LHRH Peptide. *Proc. Natl. Acad. Sci. U.S.A.* **2005,** *102*, 12962–12967.